Journal of Ocean University of China (Oceanic and Coastal Sea Research)
ISSN 1672-5182, April 30, 2005, Vol.4, No.2, pp.177-184
http://www.ouc.edu.cn/xbywb/
E-mail: xbywb@mail.ouc.edu.cn

The Application of a Numerical Model to Coastal Surface Water Waves

ZOU Huazhi*, LI Huajun, LIU Xiaodong, and LIU Aixia

College of Engineering, Ocean University of China, Qingdao 266071, *P.R. China*

(Received June 29, 2004; accepted December 10, 2004)

Abstract Based on the Navier-Stokes Equations (NSE), numerical simulation with fine grids is conducted to simulate the coastal surface wave changes, including wave generation, propagation, transformation and interactions between waves and structures. This numerical model has been tested for the generation of the desired incident waves, including both regular and random waves. Some numerical results of this model are compared with available experimental data. In order to apply this model to actual cases, boundary conditions are considered in detail for different shoreline types (beach or breakwater, slope or vertical wall, *etc.*). Finally, the utility of the model to a real coastal area is shown by applying it to a fishing port located in Shidao, Rongcheng, Shandong Province, P.R. China.

Key Words wave propagation; wave generation; numerical simulation; Navier-Stokes Equations; boundary condition

Number ISSN 1672-5182(2005)02-177-08

1 Introduction

Wave climate plays a very important role in all coastal projects. But, in most cases, little wave data are available for engineering construction and planning. On the other hand, field observations and physical modeling of waves are difficult, costly, and time-consuming. However, the desired sea-state information may be obtained and evaluated with reliable mathematical modeling techniques.

There are indeed several wave theories available that could adequately describe the combined refraction and diffraction of waves from deep to shallow waters (Demirbilek and Webster, 1998). One of these is the mild-slope equation (MSE), which is a depth-averaged, elliptic type partial differential equation which ignores evanescent modes (locally emanated waves) and assumes that the rate of change of depth and current within a wavelength is small; hence the 'mild-slope' assumption is adopted (Demirbilek and Panchang, 1998). The classical Boussinesq Equations are known to incorporate only weak dispersion and weak nonlinearity. In recent years, many new forms of Boussinesq-type equations have been developed in order to extend the range of applicability of the equations (Madsen *et al.*, 1991; Schaffer and Madsen, 1995; Zou, 1999; Zou, 2000; Feng, 2003). However, high order Boussinesq-type Equations become more and more complex. It is very difficult to solve the equations in an actual, large calculation domain with complex seabed and boundary conditions. The use of the well-known Navier-Stokes Equations would provide a good model for not only wave propagation but also wave overtopping events (Shiach *et al.*, 2003). However, numerical solvers for the fully three dimensional Navier-Stokes Equations require extensive computational resources, and it was not until computers were sufficiently developed that a model based on the Navier-Stokes Equations had become practical. In addition, all the existing wave models have great difficulty in taking coastal structures and the shoreline type into appropriate consideration (Demirbilek and Panchang, 1998; Ge *et al.*, 1999; Balas and Inan, 2002). And they are incapable of dealing with the diversity of coastal structures in form and height, which significantly affect the transform of waves.

In this study, a numerical model based on the modified Navier-Stokes Equations, which considers in detail the diversity of coastal structures, the existence of beach and different boundary conditions, is developed to simulate the process of wave propagation and run-up onto coastal regions. The applicability of the model is validated by comparisons between the numerical results and available experimental data (Berkhoff *et al.*, 1982). Furthermore, the utility of the model in real coastal areas is shown by its application to a fishing port located in Shidao, Rongcheng, Shandong Province, P.R. China.

* Corresponding author. Tel: 0086-532-5875224
E-mail: zouhuazhi@hotmail.com

2 Basic Theory

The continuity and momentum equations are as follows:

$$\frac{\partial u}{\partial x}+\frac{\partial v}{\partial y}+\frac{\partial \omega}{\partial z}=0, \tag{1}$$

$$\frac{\partial u}{\partial t}+u\frac{\partial u}{\partial x}+v\frac{\partial u}{\partial y}+\omega\frac{\partial u}{\partial z}=F_x-\frac{1}{\rho}\frac{\partial p}{\partial x}+\gamma\nabla u, \tag{2}$$

$$\frac{\partial v}{\partial t}+u\frac{\partial v}{\partial x}+v\frac{\partial v}{\partial y}+\omega\frac{\partial v}{\partial z}=F_y-\frac{1}{\rho}\frac{\partial p}{\partial y}+\gamma\nabla v, \tag{3}$$

$$\frac{\partial \omega}{\partial t}+u\frac{\partial \omega}{\partial x}+v\frac{\partial \omega}{\partial y}+\omega\frac{\partial \omega}{\partial z}=F_z-\frac{1}{\rho}\frac{\partial p}{\partial z}+\gamma\nabla \omega, \tag{4}$$

where u, v, ω, are velocities in the x, y, z directions; F_x, F_y, F_z are force components; ρ is the water density; γ the coefficient of viscosity; p the dynamical pressure; t the time. Assume that the horizontal acceleration is significant and the vertical acceleration can be neglected; accordingly, the terms on the left-hand side of Eq. (4) are set to be zero. The velocity will be eliminated, and the number of unknown variables is reduced to three. When integrating the equations with respect to z, we have:

$$\frac{\partial \eta}{\partial t}+\frac{\partial M}{\partial x}+\frac{\partial N}{\partial y}=0, \tag{5}$$

$$\frac{\partial M}{\partial t}+\frac{\partial}{\partial x}\frac{M^2}{D}+\frac{\partial}{\partial y}\frac{MN}{D}+gD\frac{\partial \eta}{\partial x}+\frac{gn^2}{D^{7/3}}M\sqrt{M^2+N^2}=0, \tag{6}$$

$$\frac{\partial N}{\partial t}+\frac{\partial}{\partial x}\frac{MN}{D}+\frac{\partial}{\partial y}\frac{N^2}{D}+gD\frac{\partial \eta}{\partial y}+\frac{gn^2}{D^{7/3}}N\sqrt{M^2+N^2}=0, \tag{7}$$

where η is the water elevation; D the total water depth ($D=h+\eta$), h still-water level; M, N are the flow fluxes in the x and y directions respectively; n is Manning's roughness coefficient and g is the gravitational acceleration.

3 Numerical Approximations and the Stability Criterion

A finite difference method is applied to solving the equations. In the computations, Eqs. (5) to (7) are formulated with a staggered difference scheme for space and a leap-frog difference scheme for time. Further, the calculations related to the nonlinear terms are performed with an up-wind difference scheme. Fig.1 shows the difference schemes used. Because of similarity, only several difference terms in these three equations are given as follows.

$$\frac{\partial \eta}{\partial t}=\frac{1}{\Delta t}\left[\eta_{i,j}^{k+1}-\eta_{i,j}^{k}\right], \tag{8}$$

$$\frac{\partial M}{\partial t}=\frac{1}{\Delta t}\left[M_{i+1/2,j}^{k+1/2}-M_{i+1/2,j}^{k-1/2}\right], \tag{9}$$

$$\frac{\partial M}{\partial t}=\frac{1}{\Delta x}\left[M_{i+1/2,j}^{k+1/2}-M_{i-1/2,j}^{k+1/2}\right], \tag{10}$$

$$\frac{\partial}{\partial x}\frac{M^2}{D}=\frac{1}{\Delta x}\left[\lambda_{11}\frac{(M_{i+3/2,j}^{k-1/2})^2}{D_{i+3/2,j}^{k-1/2}}+\lambda_{21}\frac{(M_{i+1/2,j}^{k-1/2})^2}{D_{i+1/2,j}^{k-1/2}}+\lambda_{31}\frac{(M_{i-1/2,j}^{k-1/2})^2}{D_{i-1/2,j}^{k-1/2}}\right], \tag{11}$$

$$\frac{\partial}{\partial y}\frac{MN}{D}=\frac{1}{\Delta y}\left[\gamma_{11}\frac{M_{i+1/2,j+1}^{k-1/2}N_{i+1/2,j+1}^{k-1/2}}{D_{i+1/2,j+1}^{k-1/2}}+\gamma_{21}\frac{M_{i+1/2,j}^{k-1/2}N_{i+1/2,j}^{k-1/2}}{D_{i+1/2,j}^{k-1/2}}+\gamma_{31}\frac{M_{i+1/2,j-1}^{k-1/2}N_{i+1/2,j-1}^{k-1/2}}{D_{i+1/2,j-1}^{k-1/2}}\right], \tag{12}$$

where

$$\begin{cases}\lambda_{11}=0,\ \lambda_{21}=1,\ \lambda_{31}=-1 & (M_{i+1/2,j}^{k-1/2}\geqslant 0),\\ \lambda_{11}=1,\ \lambda_{21}=-1,\ \lambda_{31}=0 & (M_{i+1/2,j}^{k-1/2}<0),\end{cases} \tag{13}$$

$$\begin{cases}\gamma_{11}=0,\ \gamma_{21}=1,\ \gamma_{31}=-1 & (N_{i+1/2,j}^{k-1/2}\geqslant 0),\\ \gamma_{11}=1,\ \gamma_{21}=-1,\ \gamma_{31}=0 & (N_{i+1/2,j}^{k-1/2}<0).\end{cases} \tag{14}$$

Stability criterion must be satisfied to make the scheme stable. Based on the stability analysis of the scheme, the following condition should be satisfied,

$$c=\frac{U\Delta t}{\Delta l}\leqslant\alpha,$$

where U is the larger value of the maximum particle velocity and wave celerity; Δl is max $(\Delta x, \Delta y)$. The value of α is 1.0 on principle, but it is often taken to be below 0.5 to ensure the accuracy and stability everywhere in the computational domain.

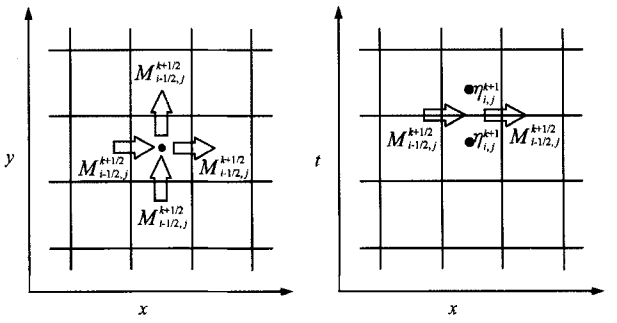

Fig.1 Difference schemes.

Since a staggered difference scheme is used for space, the line source method can work effectively and simply. The wave source in this model can be generated by a given time series of surface elevation along a line.

4 Boundary Conditions and Calculational Domain

As input data to the calculational program, the boundary conditions and calculational domain are expressed with a so-called digitized map, which consists of a series of rectangular meshes. Each mesh contains the essential calculation information such as the discrimination of a mesh (a shoreline mesh or an open sea mesh), water depth, structure shape and height, *etc.* Fig.2 shows a simple example. The first integer of the mesh code indicates the mesh type: '1' stands for structure, '8' for water and '9' for beach, *etc.* The last integer indicates the relationship between water and structure meshes. Such a digitized map can accurately express the configuration, coastal structures and the boundary of the calculational domain. And such representation can be easily recognized by the calculational program. Thus, roughness, structure shape, slope scale *etc.* can be considered respectively.

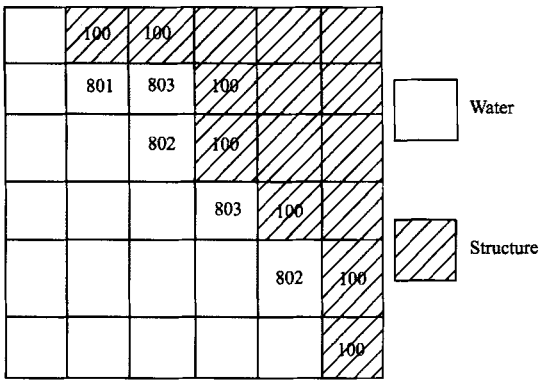

Fig.2 An example of water-structure interface.

Using an eigenvector method, open sea boundary conditions are presented for cases where outgoing waves leave the numerical domain of calculation through the open boundary. Waves are reflected in front of a structure, the reflection rate being related to its slope. In the computations, run-up and overtopping are taken into account in the boundary area. When $D = h + \eta > 0$, waves run up. When the water level of the wave rises above the height of a breakwater or a seawall, the flow flux of wave overtopping is calculated from the following Honma's equation:

when $h_2/h_1 \leqslant 2/3$, $Q = \mu h_1 \sqrt{2gh_1}$,

when $h_2/h_1 > 2/3$, $Q = \mu' h_1 \sqrt{2g(h_1 - h_2)}$,

where h_1 and h_2 are the water depths (based on the top of a structure) before and behind a structure, respectively. The coefficients $\mu = 0.35$ and $\mu' = 0.26\mu$.

5 Model Test

In this section, the line source method is used to study several cases of wave generation and propagation for both monochromatic and random waves. In all the examples, the wave source is given in terms of surface elevation $\eta(x_s, t)$.

5.1 2D Monochromatic Waves

The computational domain shown in Fig.3 is considered. The horizontal length of the domain is $L_x = 50$ m, its width $w_y = 1$ m and the water depth $h = 1$ m is constant. The wave source is located at $x_s = 25$ m. To let outgoing waves leave, the right-hand end of the domain is set to be an open boundary. The left-hand end is set to be a vertical wall. A monochromatic wave with period $T = 1$ s and amplitude $a_0 = 0.025$ m is generated at the center of the computational domain. The mesh size is $\Delta x = \Delta y = 0.02$ m, and the time step size is $\Delta t = 0.005$ s. Fig.4 shows the snapshots of the relative surface elevation expressed as η/a_0 at various times ($t/T = 5, 7.5, 10$), η being the surface elevation at sites other than the source.

It can be seen that waves are generated first along the line source at the center of the domain and then propagate towards the two ends. The open boundary at the right-hand end of domain works so as to let outgoing waves leave the numerical domain of calculation. Notice that the vertical wall at the left-hand end reflects the incident wave, and the reflected wave is in phase with the incident wave, leading to a wave with double amplitude. This is due to the fact that the distance from the wave source to the wall is 25 m, which is equivalent to 16 wave lengths. The wave crests and troughs are very close to the horizontal dashed grid lines, and the vertical distance between the crest and trough gives the relative height of the target wave. Further analysis shows that the relative error between

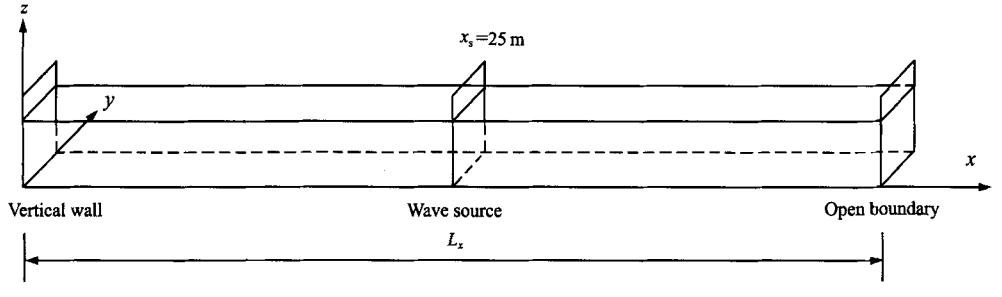

Fig.3 The computational domain layout.

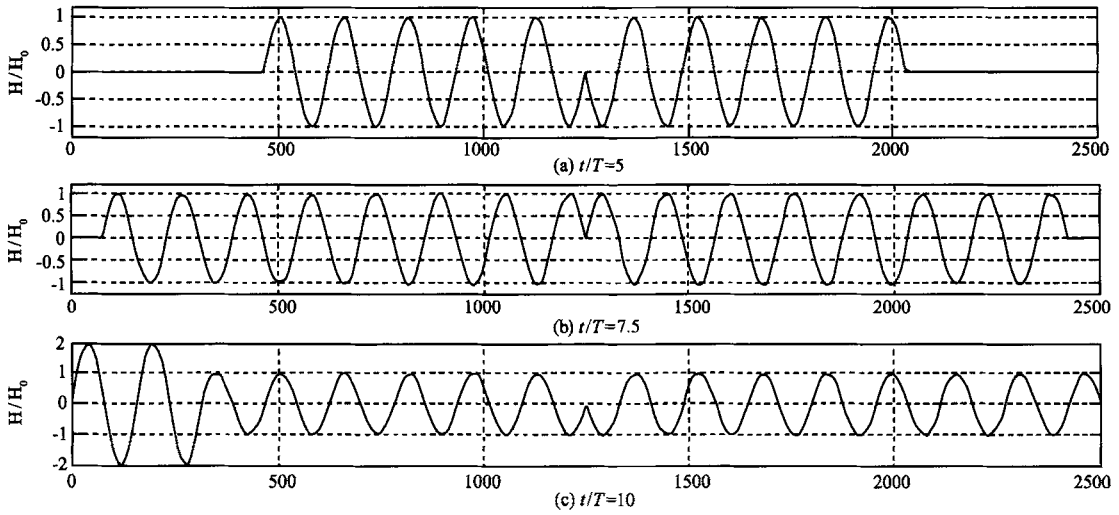

Fig.4 Snapshots of surface elevation at different times.

the target and generated wave heights is less than 0.15%.

5.2 Waves with Different Periods and Amplitudes

Next the model is utilized to generate monochromatic waves with three different periods $T = 0.5, 1, 2$ s, and three different amplitudes $a_0 = 0.0125, 0.025, 0.05$ m. All the parameters (*e.g.* water depth, domain length, grid size, time step size, wave source location) are kept the same as those in the previous example. The source line is, however, situated at the left end. The generated waves shown in Figs.5 and 6 are quite satisfactory and the corresponding wave heights are very close to their target values. These results indicate that the model can be utilized to simulate random waves which consist of superposed monochromatic wave components with different frequencies and amplitudes. Next this model is used to simulate a set of random waves. The wave source line is also set at the left-hand end, and the target time series of surface elevation is shown in Fig.7. The simulation results are shown in Figs.8 and 9. The relative error between the target and generated wave height is less than 0.3%, so the model can accurately generate and propagate random waves too.

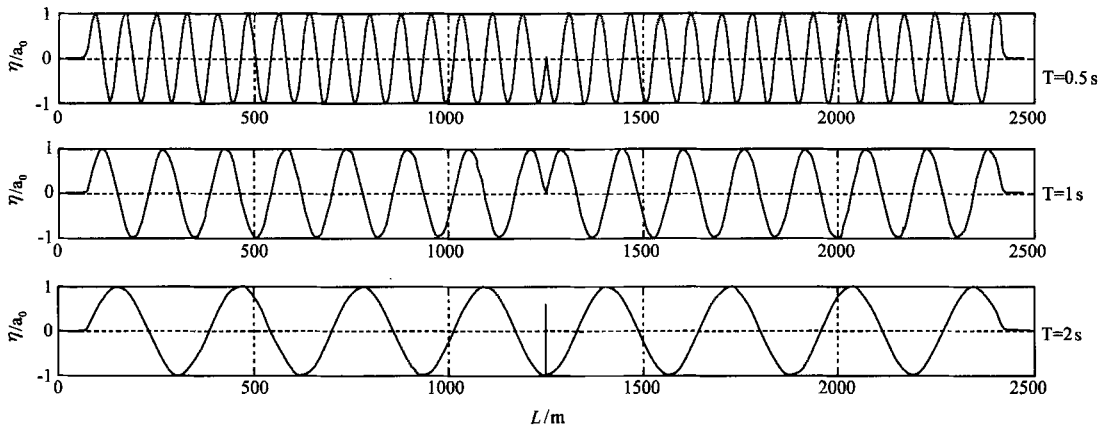

Fig.5 Waves with different periods.

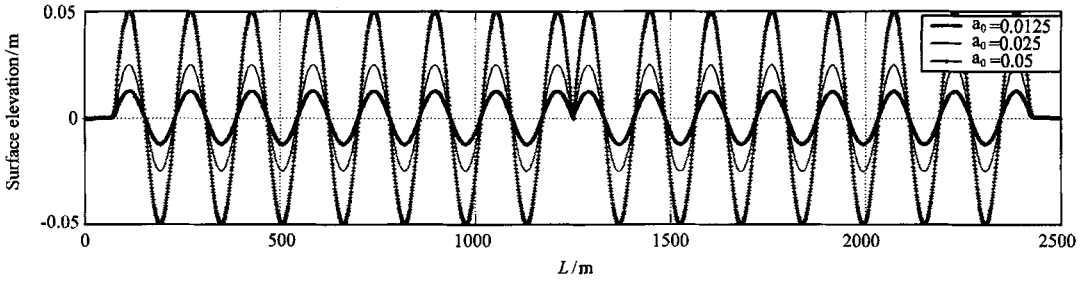

Fig.6 Waves with different amplitudes.

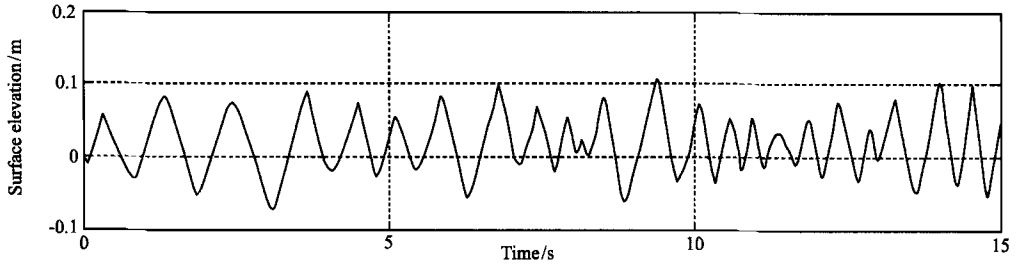

Fig.7 Target random wave source $\eta(t)$.

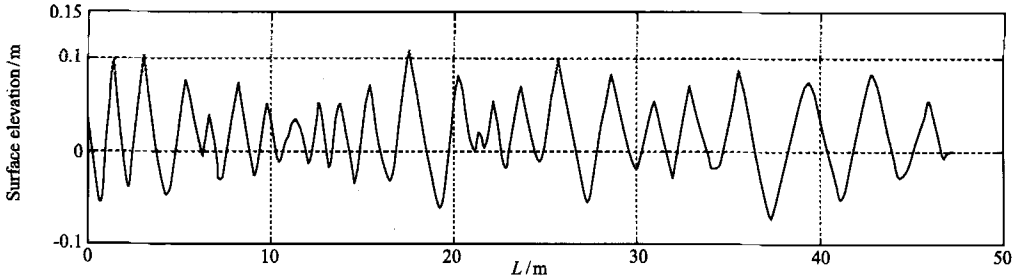

Fig.8 A snapshot of surface elevation at $t = 15$ s.

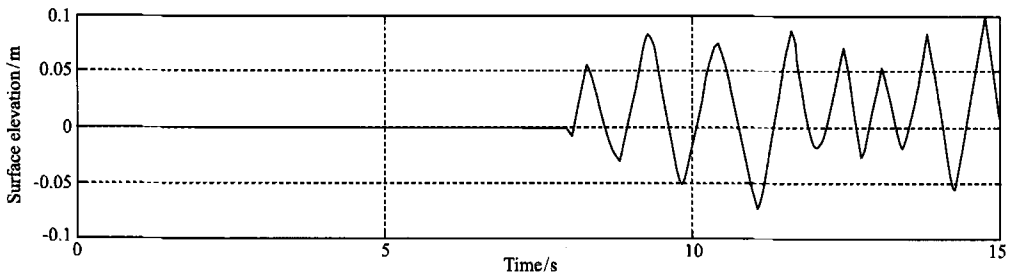

Fig.9 Surface elevation at point $x = 25$ m.

5.3 Comparison with Experiment

To illustrate the importance of wave refraction and diffraction effect over complex bathymetry, Berkhoff *et al.* (1982) conducted a laboratory study of 2D monochromatic wave propagation over a plane beach with an elliptic shoal. The experiment layout and transects for collecting wave data are shown schematically in Fig.10. Monochromatic wave with period $T = 1$ s and amplitude $\eta_0 = 2.32$ cm is generated by a wavemaker at $y = -10$ m. The bottom contours on the slope are oriented at an angle of 20°. Detailed formula for the bottom bathymetry can be found in (Berk *et al.*, 1982).

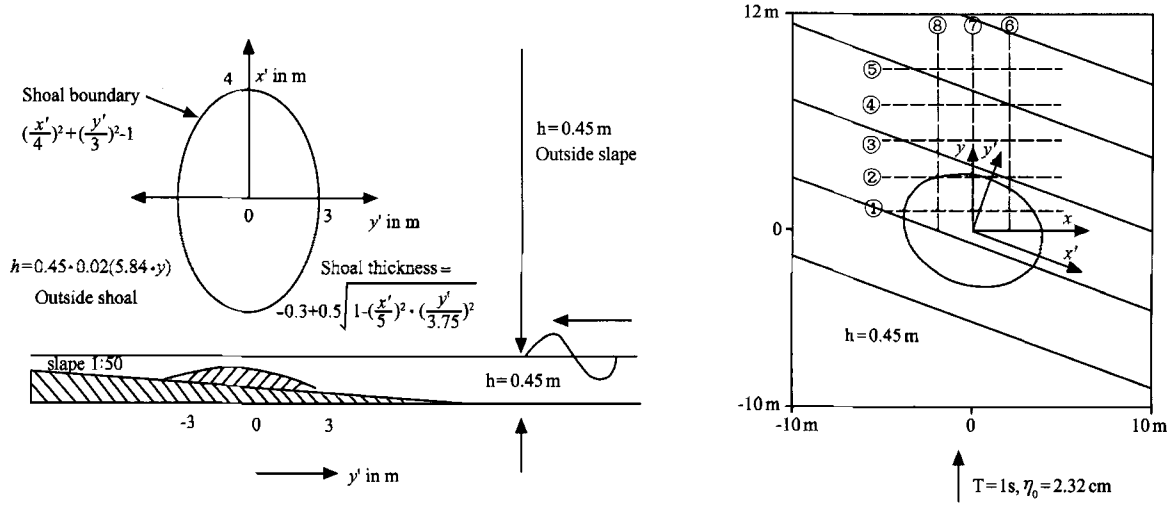

Fig.10 Layout of the experiment by Berkhoff.

To demonstrate the capability of this model to simulate the effects of complex coastal bathymetric features, the model was run up to $t = 50$ s without any stability problems on a Pentium PC with 256 MB memory and 1.8 G CPU. The mesh size used in this example was $\Delta x = \Delta y = 0.02$ m and the time step size was $\Delta t = 0.005$ s. The CPU time for solving all equations at each time step was about 1.2 s; however, it was more than 100 s when the fully three-dimensional model of Navier-Stokes Equations was used (Li and Fleming, 2001). Fig.11 shows a comparison of wave amplitudes along all the eight transects between the experimental and the model results. The wave amplitudes for the model were obtained by averaging those of four consecutive waves. The agreement is shown to be excellent.

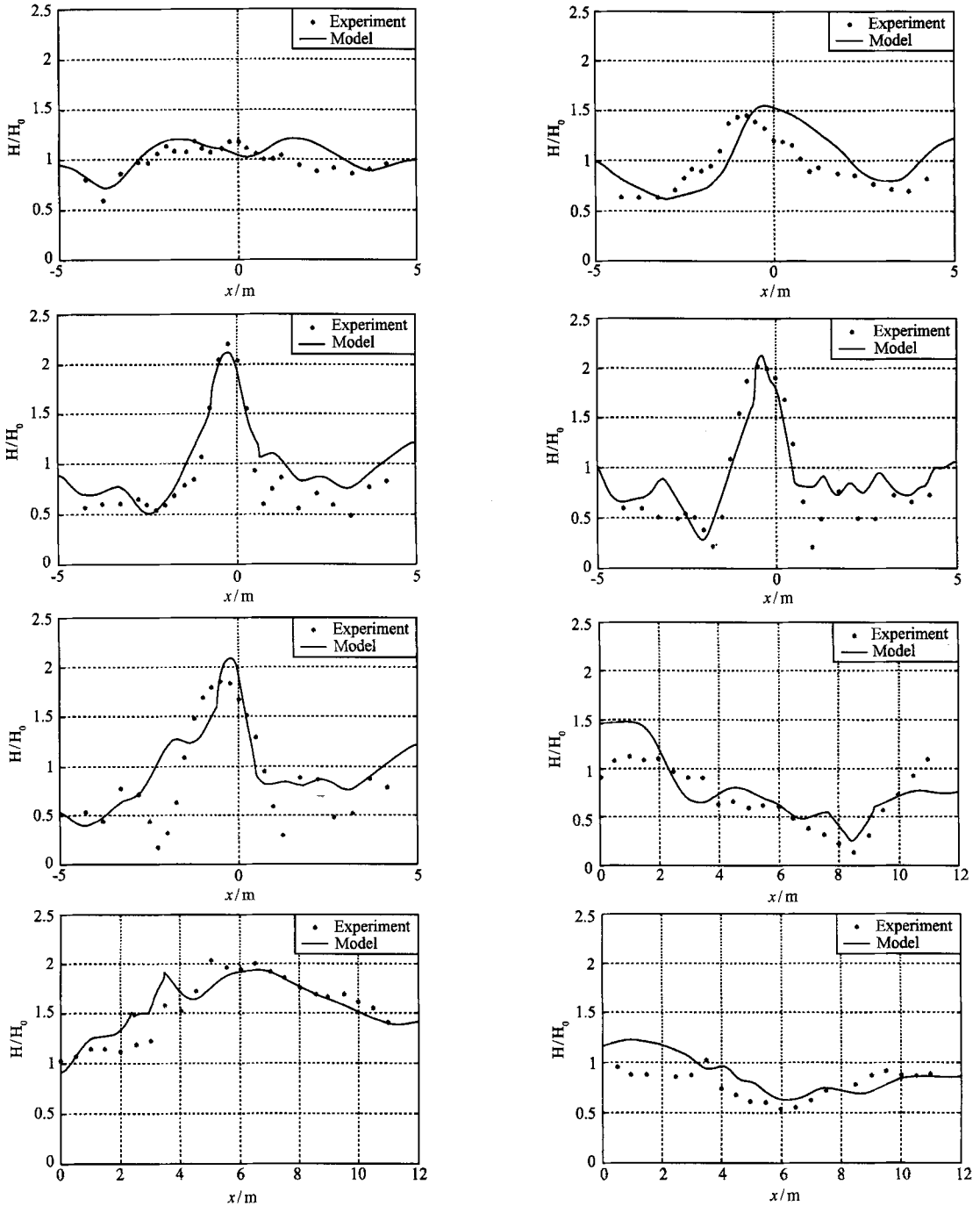

Fig.11 Comparisons of experimental and model results.

6 A Case Study

To optimize the planning design of a fishing port located in Shidao, Rongcheng, Shandong Province, P. R. China, this model is employed to simulate the water surface agitation induced by waves in this fishing port, which is part of the project of rebuilding the

Shidao Fishing Port. According to the Plane Figure of Shidao Fishing Port at 1:15 000 and the observations of water depth in this region, a digitized map is drawn.

On this map, three sets of input data, including water depth, shoreline type and the location and height of coastal structures, are prepared for mesh size 10 m by 10m for the reason that it can accurately represent the geomorphic configuration and the coastal structures in this region. The simulation region is 5.41 km by 3.97 km, thus there are 541 by 397 meshes in the calculational domain. The time step size is Δt = 0.1 s. From observations, the primary wave direction in this area is east. The designed wave height is $H_{1\%}$ = 6.4 m, and wave period T = 13.3 s. This model was run up to t = 1200 s without any stability problems by giving a monochromatic wave line source with H_0 = 6.4 m and T = 13.3 s at the right-hand boundary of the domain. An analysis of the calculation results is concentrated on the Fishing Port indicated by the rectangle in Fig.12.

From Fig.13 we can clearly see wave reflection, diffraction, refraction and the interactions between reflected waves and incident waves. The H_{max} at different transects and the water elevation history at different points (see Fig.12 for their locations) indicate that the water surface agitation inside the fishing port are smaller than those outside it due to the existence of the breakwater.

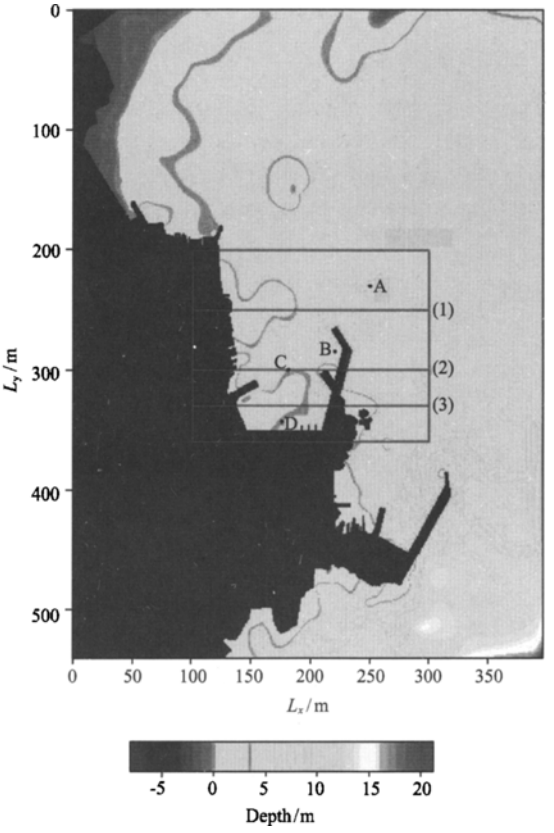

Fig.12 Layout of Shidao fishing port.

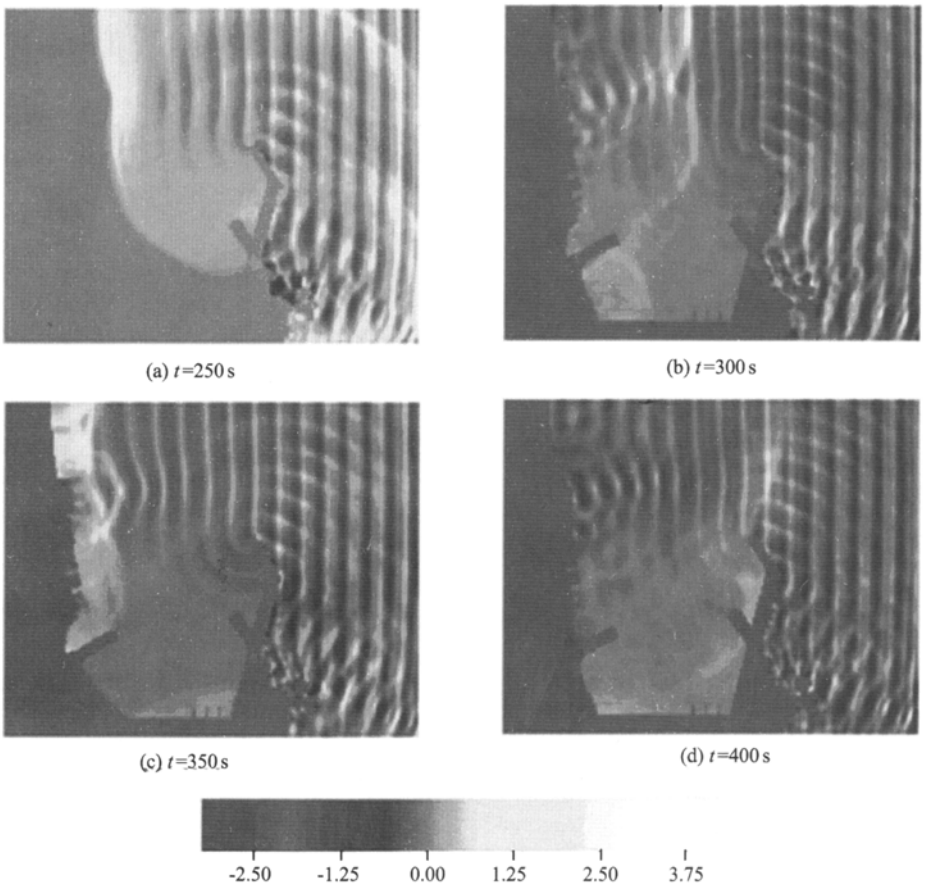

Fig.13 Top views of wave surfaces at different times.

7 Conclusions

Numerical experiments, including the case for an elliptic shoal, show that wave generation, propagation, reflection and interaction between waves and coastal structures can be successfully simulated by using the theoretical model developed in this study. The success in applying the model to a real coastal fishing port indicates its potential applicability to various coastal areas with different forms of structures. In addition, the lower CPU time consumption and memory requirement make the model can be efficiently implemented on a PC to simulate the wave propagation at larger coastal areas.

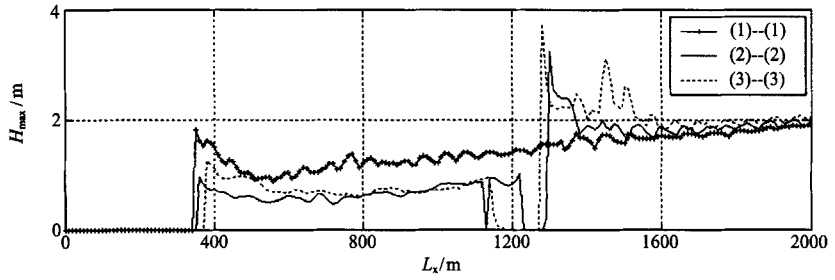

Fig.14 Distribution at different transects.

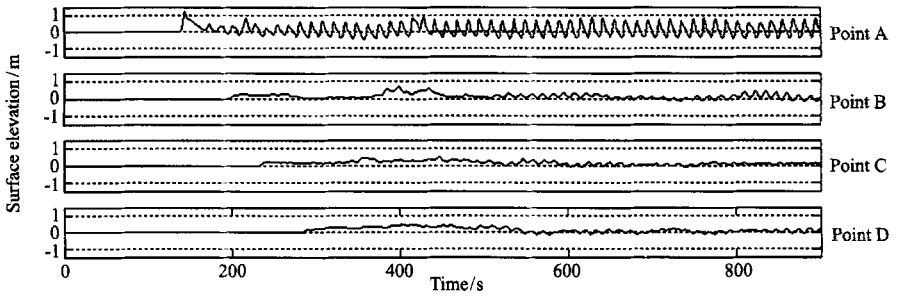

Fig.15 Surface elevation at points A, B, C, D.

Acknowledgements

This research is financially supported by the National Natural Foundation of China (No. 50479027) and the Natural Science Foundation of Qingdao (Grant No. 03-jr-15). The support is gratefully appreciated.

References

Balas, L., and A. Inan, 2002. A numerical model of wave propagation on mild slopes. *Journal of Coastal Research*, **36**: 16-21.

Berkhoff, J. C. W., N. Booy, and A. C. Radder, 1982. Verification of numerical wave propagation models for simple harmonic linear water waves. *Coastal Engineering*, **6**: 255-279.

Demirbilek, Z., and W. C. Webster, 1998. A shallow-water wave theory based on green-naghdi formulation. *Handbook of Coastal Engineering*, Vol. 4. Herbich, J. B., ed, Gulf Publ. Co, Houston, 250-256.

Demirbilek, Z., and V. Panchang, 1998. CGWAVE : A coastal surface water wave model of the mild slope equation. *Technical Report* (CHL-98-26). US Army Corps of Engineers Waterways Experiment Station, Vicksburg, Mississippi, 112 pp.

Feng, Z. S., 2003. Traveling solitary wave solutions to the generalized Boussinesq equation. *Wave Motion*, **37**: 17-23.

Ge, W., J. T. Kirby, and A. Sinha, 1999. Generation of waves in Boussinesq models using a source function method. *Coastal Engineering*, **36**: 271-299.

Li, B. B., and C. A. Fleming, 2001. Three-dimensional model of Navier-Stokes equations for water waves. *J. Wtrwy, Port, Coast. and Oc. Engrg.*, **127**: 16-25.

Madsen, P. A., R. Murray, and O. R. Sorensen, 1991. A new form of the Boussinesq equations with improved linear dispersion characteristics. *Coastal Engineering.*, **15**: 37-388.

Schaffer, H. A., and P. A. Madsen, 1995. Further enhancements of Boussinesq-type equations. *Coastal Engineering.*, **26**: 1-14.

Shiach, J. B., C. G. Mingham, D. M. Ingram, and T. Bruce, 2003. The applicability of the shallow water equations for modeling violent wave overtopping. *Coastal Engineering*, **51**: 1-15.

Zou, Z. L., 1999. Higher order Boussinesq equations. *Ocean Engineering*, **26**: 767-792.

Zou, Z. L., 2000. A new form of higher order Boussinesq eqations. *Ocean Engineering*, **27**: 557-575.